

tissues. The reference state is a tube of infinite length and radius r_0 . We first discuss a peristaltic perturbation (varicose, or pearling) which respects the cylindrical symmetry. The displacements can therefore be written $(u_r(z), u_z(z))$ where z is the coordinate along the tube and r the radial direction. The forces involved are equivalent to those derived from the following effective energy [13]:

$$\frac{\mathcal{E}_{el}}{2\pi r_0} = \frac{E_t h}{2} \int (e_z^2 + e_\theta^2 + 2\nu e_z e_\theta) dz + \frac{K}{2} \int \left(\mathcal{C} - \frac{1}{r_0} \right)^2 dz \quad (1)$$

where ν is the Poisson ratio, and the strains are defined as

$$e_\theta = \frac{u_r}{r_0} + \frac{1}{2} \left(\frac{u_r}{r_0} \right)^2; e_z = u'_z + \frac{1}{2} (u'_r{}^2 + u'_z{}^2) \quad (2)$$

where the prime denotes a derivative with respect to z . The first term is the stretching elastic energy of the tube. We use here the classical Foppl-Von Karman approximation [13], neglecting $u'_z{}^2$, but we keep the nonlinear term $(\frac{u_r}{r_0})^2$, if uniform dilations of the tube are non-negligible. The second term is the layer bending energy where \mathcal{C} is the local curvature, and $K = \frac{E_t h^3}{12(1-\nu^2)}$ the bending modulus. A key difference with Ref. [14] is that we do not assume that the outer surface of the cylinder is fixed. The case of arteries is complicated by the presence of smooth muscles and anisotropy but as we wish to capture the essential physics, we restrain ourselves to this simple nonlinear and isotropic elastic theory. Surface and pressure forces, which drive the deformation, are derived from an effective energy in which the non-equilibrium aspect is hidden in the surface tension and excess pressure terms:

$$\mathcal{E}_a = \int (2\pi\gamma(r_0 + u_r(z))\sqrt{1 + u'_r{}^2} - \pi\Delta P(r_0 + u_r(z))^2) dz \quad (3)$$

where γ is the effective surface tension, which contains a negative contribution due to cell division. As a result, γ can be positive or negative. ΔP is an excess pressure inside the tube. We first investigate a deformation of the tube to a radius $u_r(z) = r_0[R_0 - 1 + A \cos(kz)]$ which includes both a uniform dilation to a radius $R_0 r_0$ and a pearling deformation of amplitude $A r_0 \ll r_0$. All lengths have been normalized by r_0 (see SI for details). We first discuss the effect of negative surface tension, assuming that there is a small excess pressure, $\Delta P r_0 \ll |\gamma|(h/r_0)^2$. Compared to the classical Rayleigh-Plateau instability, the wavelength observed in vivo is small, close to the value of the tube radius [2, 6, 15]. We propose that this pearling instability is due to a buckling of the tube induced by the homeostatic pressure of the dividing epithelial cells. This hypothesis has biological grounds for hepatic arteries, since varicosities are associated with Fibromuscular Dysplasia (FMD)[15–17] or polycystic disorders in renal canals [18].

In the following, we assume that the value of the tension is such that $\frac{h^2}{r_0^2} \ll \frac{|\gamma|}{E_t h} \ll 1$, which seems to be the case for reasonable values of the parameters : tubes we will study have $\frac{h^2}{r_0^2} \approx 0.01$, and as we will discuss below, $\frac{|\gamma|}{E_t h} \approx 0.1$. The minimization of the energy with respect to R_0 leads to $R_0 = 1 + \frac{|\gamma|}{E_t h} \simeq 1$. In this limit, there is a bifurcation from tubular to pearling states for

$$|\gamma| > \gamma_p = E_t h \frac{h}{\sqrt{3}r_0} \quad (4)$$

at a wavelength $\lambda_p = 2\pi r_0 \left(\frac{1}{1-\nu^2} \frac{h}{\sqrt{12}r_0} \right)^{\frac{1}{2}}$. The finite elasticity of the surrounding medium does not change these equations as long as its modulus E_s is such that $E_s r_0 \ll E_t h$, which is the case here. The Poisson modulus ν only has a weak effect. We have performed a numerical minimization and Fig.2 shows a plot of the resulting shape of a tube that has undergone a pearling instability. For large arteries such as the common hepatic artery, the wall to lumen ratio is approximately $\frac{h}{r_0} = 0.1$, so that $\lambda_p \approx 1.1r_0$. Strikingly, clinical studies [16] confirm that the size of the pattern is proportional to the radius of the artery, with the exact same coefficient as above, in contradiction to analyses based on the Rayleigh-Plateau instability [19].

Away from the bifurcation point, the wavelength varies only slowly. This variation is compatible with the biological variability, and explains why the same range of wavelengths is always observed. Since the wavelength is of the order of the radius, we need not consider instabilities in the section plane of the tube, studied in Ref. [20]. For much thinner tubes, such an analysis would be required. The negative tension exerted by the cells is linked to the homeostatic pressure, $\gamma \approx -P_h h$ [21]. Pressure measurements for tumors or dysplasia often give values in the range of $P_h = 10^4 Pa$ [22]. Taking $E_t = 10^5 Pa$, the critical tension $\gamma_p \approx 7.10^3 h$ is perfectly compatible with a buckling induced by the dividing cells.

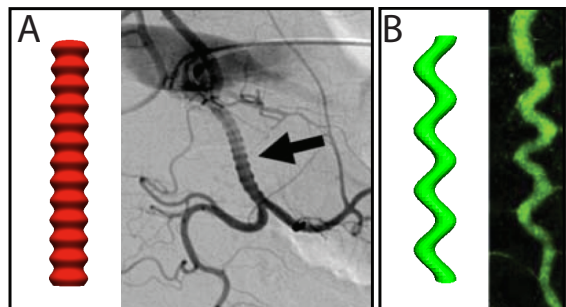


FIG. 2. Comparison between the shapes obtained from buckling theory and in vivo data. A: a common hepatic artery displaying varicosities [15]. B: a drosophila tracheal tube displaying sinusoidal mutation [23], $\lambda \approx 5r_0$.

Polycystic diseases are more complex. The tubular canals of the kidney lose their stability, giving rise to

a variety of patterns : string of small pearls, large convolutions, or huge spheric cysts that can invade the entire organ [6] [24]. Three main factors [18] have been identified : increase in basement membrane compliance, uncontrolled division of the epithelial cells forming the tube wall, and disorders in ions pumps, causing excess water to be pumped in the canals. In our formalism, this relates respectively to a decrease in E_t , an increase in P_h , and an increase in ΔP . The excretory canal of *C. Elegans* is often used as a model organism to study these diseases. Although the tube is different in nature [25] (a single, elongated cell invaginates to form a tube which spans its entire length), it can be described by similar equations : there is a bending energy associated to membrane deformation, a surrounding elastic medium prevents stretching, the tube can grow because of excessive lipid transport, analogous to negative surface tension, and there can exist hydrostatic pressure differences. Thus, in order to incorporate the effect of pressure differences, we now consider the opposite limit of enlarged tubes, where the pressure dominates over tension effects, $\Delta P r_0 \gg |\gamma|(h/r_0)^2$. The equilibrium radius is such that the elastic deformation equilibrates the excess pressure.

$$R_0 = \left(1 + 2 \frac{\Delta P r_0}{E_t} \frac{r_0}{h}\right)^{1/2} \quad (5)$$

The physical picture of pearling is not modified greatly by considering the effect of an excess pressure. The threshold tension remains of the same order, and the characteristic undulation wavelength is slightly reduced : $\lambda_p = \lambda_p(\Delta P = 0)(1 + 5\Delta P r_0/3E_t h)^{-1/4}$.

We then turn to sinusoidal oscillations of the entire tube. The classical Euler buckling instability of an elastic column under compression occurs at a wavelength which is the system size, in the absence of a surrounding elastic medium. However, in an elastic medium, buckling occurs at a finite wavelength. We have shown recently that this instability can be invoked to describe the morphology of the intestine [26].

We call E_t and E_s respectively the Young moduli of the tube and surrounding elastic medium, keeping in mind that $E_t \gg E_s$. We denote the deformation of the tube by $w(z, t) = B \cos(kz)$. The curvature modulus of a hollow elastic tube is $K = \pi E_t r_0^3 h$, the force exerted by the growing tube is $f = 2\pi\gamma r_0$, and the elastic force exerted by the surrounding medium is proportional to the deformation with a coefficient α . The threshold force of the sinusoidal instability is $f = 2\sqrt{K\alpha}$, thus the critical tension for buckling is

$$|\gamma| > \gamma_s \approx 0.8\sqrt{r_0 h} \sqrt{E_s E_t} \quad (6)$$

The wavelength of the instability is $\lambda_s = 2\pi r_0 (\frac{h}{2r_0} \frac{E_t}{E_s})^{1/4}$. A rough estimate leads to $\lambda_c \approx 5 - 10 r_0$, in agreement with observations of degenerate excretory canals in *C. Elegans* [6], or of the tracheal system in drosophila ([2] and Fig.2).

We now compare sinusoidal deformations, which occur for cell tensions larger than γ_s given by Eq.(6), with pearling deformations with a threshold γ_p given by Eq.(4). The preferred morphology essentially depends on the value of the parameter $r = \frac{E_s r_0^3}{E_t h^3}$. If the substrate is very soft or the tube very hard, the sinuous morphology is expected, since in that case, it requires a smaller tension. Conversely, if $\frac{h}{r_0}$ is very small, the pearling instability is expected. Physically, this is due to the fact that a larger tube is harder to bend than a thicker tube : its curvature modulus varies as the cube of the radius and as the first power of thickness. For a typical tube, $\frac{h}{r_0} = 0.1$, and $E_t = 10^5 Pa$, the critical substrate rigidity separating both morphologies is $E_s = 10^2 Pa$. This analysis is important since a loss of tubular rigidity is one of the causes of cystic diseases. The situation is much more complex if the substrate is modeled as viscoelastic. Over long timescales, sinuous deformations are always expected, but can be kinetically constrained. A detailed discussion goes beyond the scope of this paper[27].

In the region where both instabilities can be observed, it is necessary to compare the energies of the two configurations. We plot in thick green the transition line between the two instabilities, in the vicinity of the critical point.

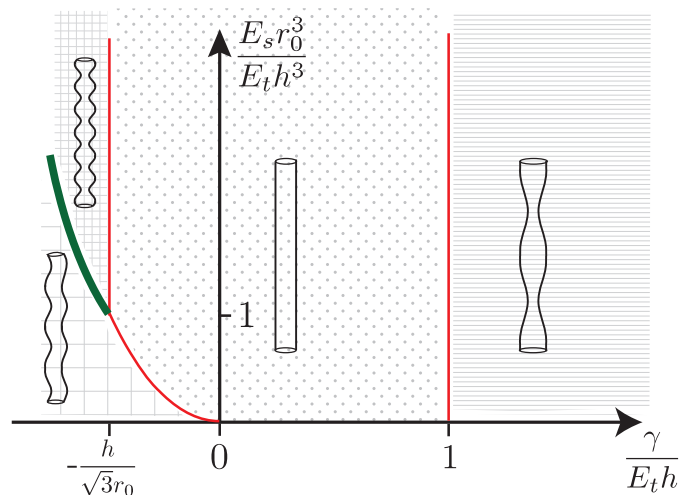


FIG. 3. Stability diagram of all possible configurations of a tube, depending on the relevant parameters. The vertical axis is the ratio of the moduli of the surrounding tissue and of the tube. The horizontal axis is the ratio of the tension, negative or positive, and the elasticity of the tube. Lines in thin red represent the transition to an instability. The thick green line separates stability domains of the varicose and sinuous patterns.

The results are displayed on a stability diagram in Fig.3. The drosophila tracheal system would be a good candidate for putting this theory to the test. It has been widely studied as a model of tube size regulation and the deletion of several genes has been identified to cause

pathologies. Specifically, mutants lacking the Sinuous, or Varicose genes respectively display sinuous [28], and pearling state morphologies [29]. Although we do not have a good understanding of their roles, it is known that they are required in cell-cell junctions (associated to the rigidity of the tube) and that they have a role in controlling growth. We now show how our phase diagram could guide further experiments. The modulus of the normal tracheal wall was inferred from experiments to be around $20kPa$ [30], and $\frac{h}{r_0} \approx 0.2$. Although tracheal connective tissue has not been probed, usual orders of magnitude are $100Pa$. In normal organisms, the relevant ratio therefore is $\frac{E_s r_0^3}{E_t h^3} = 0.6 < 1$, so sinusoidal instabilities are expected. Nevertheless, disturbing junctions lowers the rigidity of the tube, and a three-fold decrease in E_t would cause the pearling instability to be favored. We therefore suggest that more emphasis should be put on measuring each gene influence on the mechanical properties of cellular tubes.

A last situation to address is a tube in the absence of any dysplasia of the cell wall. The surface tension is then positive. In this regime, we expect either a stable tube, or a classical Rayleigh-Plateau instability of an elastic cylinder. This is slightly different from the situation encountered in membrane tubes [11], since the fluid cylinder is surrounded by an elastic shell.

We study a perturbation $u_r(z) = r_0[(R_0 - 1) + A \cos(kz)]$. The situation that we wish to discuss does not involve any cell growth, and the instability thus occurs on a time scale small enough volume conservation is a reasonable assumption. This imposes that $R_0^2 - 1 = -\frac{A^2}{2}$. Minimizing the energy with respect to A (SI) yields a finite value of A only for a tension larger than the critical value $\gamma_r = E_t h \frac{1-\nu^2}{1-q^2}$. Below this critical value of the tension, the cylinder is stable. The instability first occurs for the longest wavelength mode $q \rightarrow 0$. Determining the exact most unstable wavelength requires a non-linear analysis, which is beyond the scope of this paper.

Nevertheless, if the size of the perturbation approaches the radius of the tube, disconnected pearls are obtained and the most unstable wavelength can be found by studying the dynamics of the perturbation u_z . The continuity equation and a Poiseuille approximation for the flow lead at lowest order to: $\frac{\partial u_z}{\partial t} = r_0^4 / (16\eta) \partial_z^2 P$ where η the fluid viscosity. The hydrostatic pressure P is calculated from the force-balance equation on the membrane $P \propto (\gamma A(-q^2 + 1) - E_t h(1 - \nu^2)A) \cos(qz)$. The most unstable wavenumber is then $q_r^2 = \frac{\gamma - E_t h(1 - \nu^2)}{2\gamma}$. This is an explanation similar to [19] for the sausage-like pattern observed on some arteries. Indeed it has been shown [31] that a very soft elastic cylinder can undergo a classical Rayleigh-Plateau instability. Testing the case of hollow elastic tubes in the same fashion could be an experimental confirmation to our theory. As expected, if

$\gamma/E_t h \gg 1$, the most unstable wavevector converges to the wavevector of the classical Rayleigh-Plateau instability $q_{RP} = \frac{1}{\sqrt{2}}$ [10].

The main result of this paper is the stability diagram, sketched on Fig.3 presenting the stabilities of most morphologies found in cellular tubes, depending of their mechanical properties. Buckling theory is in good quantitative agreement with the in vivo data. We have here deliberately used simple models for the mechanics of the tubes, to emphasize the generality of our results, and the relevance of a few dimensionless ratios to predict the observed instabilities. Most importantly, we want to stress the fact that tissues' shapes could turn out to be a meaningful criterion to detect the causes of specific pathologies. For example, in the case of excretory kidney canals, dysplasia leads to a different instability than fluid accumulation. More work is clearly needed in each specific case, but we do not expect the basic physics presented in this paper to be modified.

-
- [1] M. Affolter *et al.*, Dev Cell, Vol. 4, 1118, (2003)
 - [2] G. J. Beitel *et al.*, Development 127, 3271-3282 (2000)
 - [3] M.A. Baer *et al.*, Curr Top Dev Biol, Vol. 89 (2009)
 - [4] D. J. Andrew, A. J. Ewald, Dev Biol 341,3455, (2010)
 - [5] B. Lubarsky, M. A. Krasnow, Cell, Vol. 112, 19-28 (2003)
 - [6] M. Buechner *et al.* Dev Biol 214, 227-241 (1999)
 - [7] B. Shraiman, P Natl Acad Sci USA, 102:3318-3323 (2005)
 - [8] T. Mammoto *et al.*, Development 137:1407-1420 (2010)
 - [9] J. Ranft *et al.*, P Natl Acad Sci USA, 107, 20863 (2010)
 - [10] Lord Rayleigh, Philos. Mag. 34, 145 (1892).
 - [11] R Bar-Ziv and E. Moses, Phys. Rev. Lett., 73, 10 (1994)
 - [12] S. Laurent *et al.*, Arterioscler Thromb Vasc Bio, 14:1223-131 (1994)
 - [13] S. Timoshenko, J.M. Gere, Theory of Elastic Stability, second ed. MacGraw-Hill, New York (1961).
 - [14] P. Ciarletta *et al.*, J. Mech. Phys. Solids, 60 525-537 (2012)
 - [15] B. Peynircioglu and B. E. Cil, Cardiovasc Intervent Radiol, 31:S38-S40 (2008)
 - [16] P. F. J. New, Am Roentgen Ray Soc, 97-1, 488-499 (1966)
 - [17] P.-F. Plouin *et al.*, Orphanet Journal of Rare Diseases, 2:28 (2007)
 - [18] L. W. Welling, Pathogenesis of cysts and cystic kidneys. In The Cystic Kidney (K. D. Gardner and J. Bernstein, Eds.), 99-116. Kluwer, Amsterdam, Netherlands (1990)
 - [19] P. Alstrom *et al.*, Phys. Rev. Lett, 82, 9 (1999)
 - [20] J. Yin *et al.*, P Natl Acad Sci USA, 105,19132 (2008)
 - [21] M. Basan *et al.*, HFSP Journal, 3(4):265-272 (2009)
 - [22] G. Helmlinger *et al.*, Nat Med 3, 177- 82 (2007)
 - [23] P. Laprise *et al.*, Curr Biol 12; 20(1): 55 (2010)
 - [24] A. P. Evan, J. A. McAteer, Cyst cells and cyst walls. In The Cystic Kidney (K. D. Gardner and J. Bernstein, Eds.), pp. 2142. Kluwer, Amsterdam, Netherlands (1990)
 - [25] F. K. Nelson *et al.*, J. Ultrastruct. Res. 82, 156171 (1983)
 - [26] E. Hannezo *et al.*, Phys. Rev. Lett. 107, 078104 (2011)
 - [27] R. Huang, J. Mech. Phys. Solids, 53, 63-89 (2005)
 - [28] V. M. Wu *et al.*, J Cell Biol, Vol 164-2 (2004)
 - [29] V. M. Wu *et al.*, Development 134, 999-1009 (2007)

- [30] A.M. Cheshire et al, *Dev Dyn* 237:1874-2888 (2008)
- [31] S. Mora et al, *Phys. Rev. Lett.* 105, 214301 (2011)